U.S. Department of Commerce
National Oceanic and Atmospheric Administration
National Weather Service
National Centers for Environmental Prediction

Office Note 466

Introduction to A New Fog Diagnostic Scheme

Binbin Zhou*

Environmental Modeling Center, NCEP, Camp Springs, Maryland

May 31, 2011

---

* *Correspondent author email: Binbin.Zhou@noaa.gov*

Abstract

Conventional fog prediction is based on the surface visibility threshold "< 1000m", which is computed solely from the surface cloud liquid water content (*LWC*), in a model post processor. Because no fog physical processes are involved in the cloud schemes of current NCEP operational models, the surface cloud *LWC* is generally not reliable enough to represent fog *LWC*. As a result, this method shows very poor skill in fog prediction by current operational models. Recently a so-called multi-rule based fog diagnostic scheme, which considers several fog-related variables near the surface, is suggested and has shown a significant improvement in fog prediction. However, the drawback of the multi-rule based fog diagnosis is that it only predicts fog occurrence, not fog *LWC* or intensity. Thus, no fog visibility can be predicted from this method. To improve this, a new fog diagnostic scheme, based on an asymptotic analytical study of radiation fog (Zhou and Ferrier 2008, ZF08), is proposed. ZF08 revealed that there exists a critical turbulence threshold to control the balance and persistence of radiation fog. Besides saturation and cooling conditions, turbulence intensity is necessary for fog formation and persistence. Only when turbulence intensity near the ground is weaker than this critical threshold inside a fog, can it be stable and persist. Otherwise the fog can not form or will soon be dispersed even if it has formed. ZF08 also obtained a *LWC* vertical distribution formulation for radiation fog, based on which fog occurrence or persistence can be conveniently diagnosed in a model post processor. This office note presents a brief description of how to apply the formulation from ZF08 to develop a new fog diagnostic scheme in a model post processor. For radiation fog, the input data for this new scheme are those basic grid-point variables output from an operational model, including temperature, relative humidity, and wind speeds at the surface and high levels. To extend this scheme to other types of fog, cloud base, top and moisture horizontal advection are included. Since the *LWC* vertical distribution formulation involves several important fog physical processes, the *LWC* near the ground as well as the surface visibility computed from this scheme are more representative than those directly from operational models. In comparison to the multi-rule fog diagnostic method, the new fog scheme has following advantages: (1) it can predict fog *LWC* as well as visibility; (2) it detects fog condition based not only on variables at surface, but also on those variables at multiple levels, which is believed to be critical to reduce false alarms in many cases; (3) it still can obtain the fog *LWC* even if the *RH* values at lowest levels are less than 100%, which is an efficient way to correct model bias in fog prediction; and (4) in case of extremely low temperature as ice fog may happen, the saturation *RH* threshold with reference to ice is used. Two different types of fog events, a warm fog event in Gulf coast and an ice fog event in Yellowknife, Canada are used to validate the new scheme on fog prediction. Finally, the errors and uncertainties of this scheme are discussed.

1. Introduction

Fog is a hazardous weather but its prediction has long been a challenge for operational forecast at a weather center like NCEP. Current fog prediction from the NCEP mesoscale models and the Short Range Ensemble Forecast system (SREF) still shows a much lower performance as compared with precipitation prediction from the same models (Zhou et al. 2011). The first reason for this is a lack of appropriate fog physics in current operational models. It is well known that in operational models cloud schemes are designed for higher level cloud and precipitation instead of fog near the ground. Many important processes in fog, e.g. gravitational settling onto the ground, surface layer turbulence, etc, are not considered in these cloud schemes. The second reason is too coarse model resolution of current operational models. Since fog is a local weather which is highly influenced by local atmosphere status, terrains and small-scale drift. These local factors can not be appropriately represented by a coarse-grid model. The third reason is that operational fog forecast is generally not directly conducted within a numerical weather prediction model but diagnosed by a model post-processor. It is true that there have been many well-performed 1D, 2D and 3D fog models (e.g. Musson-Genon 1987, Bott at al. 1990, Duynkerke 1991, Bergot and Guedalia 1994, Nakanishi 2000, Pagowski et al. 2004, Müller et al. 2005, Shi et al. 2010), but these models are rarely run routinely at a weather center due to very high running and maintenance cost. Many sophisticated model simulations have revealed that the evolution of fog is extremely complicated, particularly related to turbulence (Roach et al. 1976, Welch et al. 1986, Stull 1988, Van der Velde et al. 2010). Such subtle impacts of turbulence on fog, in general, can not be well represented properly in a model post processor. For this reason, development of fog diagnostic method in a model post processor has been a major task for fog prediction at NCEP.

There have been two diagnostic schemes already implemented in the NCEP model post processor. The first one is the visibility diagnosis method. According to the definition by WMO, fog is a surface weather condition and defined when surface visibility is less than 1000 m. Thus, the forecast visibility (which is also diagnosed in the post processor) is naturally used as a reference for fog prediction. The visibility computation in NCEP's North American Mesoscale model (NAM), as well as other operational models, is based on the scheme of Stoelinga and Warner (1999). In this scheme the grid-wide visibility range is computed from

4 hydrometeors near the surface, including rain, snow, mixing phase of rain and ice pellet, and fog. In situation of fog, the Kunkel (1982) fog visibility formulation (only *LWC* near the surface is related in this method) is applied. Since all of other three hydro-meteors besides fog may also cause the visibility less than 1000m, the diagnosed fog with the visibility threshold less than 1000m may not only be caused by fog, but also by any other hydro-meteors. According to the verifications over East China and North America for both single model and the NCEP SREF, the performance of visibility-diagnosis method is consistently low (Zhou and Du 2010, Zhou et al. 2011), although an application of ensemble can improve its performance.

Given the fact that the *LWC* of fog is not well resolved by current weather operational models, the second, so-called "multi-rule" fog diagnosis, was developed to improve the visibility-diagnosis method (Zhou and Du 2010). The multi-rule fog diagnosis includes a *LWC* (or visibility) rule, a cloud base/top rule, and a surface *RH*-wind rule. With a certain threshold for each rule, the grid-wide fog occurrence binary (yes or no) forecast can be conducted in a model post based on the model outputs. The advantage of the rule-based fog diagnostic method is that it can deal with different types of fog, particularly radiation fog. The *LWC* or visibility rule, with $LWC > 0.016$ g/kg or visibility < 1000m, deals with general fog cases, which is actually the first method as discussed in the previous paragraph. The cloud rule, with cloud base < 40m and cloud top < 400m, detects the low stratus or stratus-subsidence related fog. The *RH*-wind rule, with 2m $RH > 90\sim95\%$ and 10m wind speed < 2 m/s, diagnoses radiation-related fog. The evaluation has shown that the *RH*-wind rule has the biggest contribution, at least 50% , to the total forecast skill score (Zhou and Du 2010). This means that a detection of radiation-related fog is critical to a successful fog prediction in a model post processor. As a result, the forecast with the rule based scheme outperforms that with the visibility-diagnosis by over 100% in many cases.

Nevertheless, the rule based fog scheme only diagnoses the fog condition under which fog occurs or not. In other words, it can only predict yes or no occurrence of fog, not the intensity of fog. In an attempt to predict fog intensity (or fog *LWC*, based on which visibility is computed), third method, based on the asymptotic *LWC* vertical distribution formulation of radiation fog by Zhou and Ferrier (2008), was developed. The fog *LWC* vertical distribution formulation shows that evolution (formation, development, persistence and dissipation) of a fog depends on a balance among cooling, turbulence and droplet settling onto the ground. Such

a balance inside a fog can be quantitatively addressed by a critical turbulent exchange coefficient K_c. In mathematics, K_c is proportional to cooling rate and fog depth (if fog has formed) or depth of saturated air layer near the surface (if fog has not formed). If the turbulence intensity near the ground is less than this critical value, fog can form and persist. Otherwise, fog can not form or if fog has formed, the balance inside the fog will be broken, leading to dissipation of the fog. Based on this theory, a new fog diagnostic scheme is proposed. Besides its capability of computing fog *LWC*, second advantage of this new scheme over the rule-based fog diagnosis scheme is that the new scheme diagnoses fog not only through the *RH* at the surface, but also through *RH* profiles in multiple levels. Ignoring the humidity vertical distribution, a fog prediction may lead to a significantly high false alarm rate because in many cases fog probably does not form in a saturated environment as long as the humidity decreases along the vertical direction (Petterssen 1940). With the fog *LWC* asymptotic vertical distribution formulation, fog diagnosis can be easily performed in a model post processor by checking model output *RH* and wind at both ground and multiple levels. It is noted that the formulation of Zhou and Ferrier (2008) is for radiation fog. To extend this formulation to advection and stratus-subsidence related fogs, it is enhanced by adding moist advection term and surface cloud layer. That is, keep the cloud rule in this scheme. In other words, in case of low stratus cloud with its depth less than 400 m, the cloud top is assumed as fog depth for computing the surface cloud *LWC*. Taking the model *LWC* of the surface cloud as a first guess, the surface cloud *LWC* (i.e. fog *LWC*) is re-computed through the asymptotic fog *LWC* vertical distribution formulation. Third advantage of the new scheme is that it can calculate fog *LWC* even when the surface *RH* does not reach 100%. It is a common experience for local forecasters that in many cases fog has appeared but model *RH* near the surface is still less than 100%, due partly to model bias. This can be adjusted through assuming a *RH* threshold less than 100%, e.g. 95%. With such a less-than 100% threshold from the ground to upper levels, fog layer can be determined from the *RH* profile and its *LWC* can be easily computed with the fog *LWC* asymptotic vertical distribution formulation.

This office note is organized as following: Section 2 is a brief description of the asymptotic fog *LWC* vertical distribution formulation, based on which persistence condition of fog and its extension to advection types of fog and low stratus will be discussed; Section 3 is a description of computation steps and procedures, Section 4 is a brief discussion of accuracy of the scheme;

section 5 presents some testing examples; Section 6 and 7 show validations of 2 fog predictions with the new scheme using data from NCEP operational models, one for a warm regional fog event along the Gulf coast, and the other for an ice fog event in Yellowknife of Canada followed by last section of summary.

2. Theoretic background

2.1 Case without advection

In a model post processor, all of variables and products are diagnosed under an assumption of steady or quasi-steady condition of the atmosphere. In a steady and horizontally uniform radiation fog, the vertical distribution of *LWC* can be expressed as following one-dimensional (1D), second-order ordinary differential equation for boundary condition problem (ODE, ZF08),

$$\begin{aligned} &K\frac{d^2W}{dz^2}+2\alpha W\frac{dW}{dz}+\beta(T,p)C_o(z)=0, \\ &W(0)=0, W(H_{sat})=0, \end{aligned} \qquad (1)$$

where W is the *LWC* in $\mathrm{g}\,kg^{-1}$, K the turbulent exchange coefficient (m^2s^{-1}), z the vertical height, α the gravitational settling parameter (for radiation fog, $\alpha=0.062$, a gravitational settling constant parameter suggested by Brown and Roach (1976)), T and p the air temperature and pressure, respectively, H_{sat} the fog depth or surface saturated layer depth if fog has not formed yet, and $C_o(z)=-(\partial T/\partial t)$ the total local cooling rate (positive for cooling while negative for warming), hereafter referred to as cooling rate. Then the term $\beta(p,T)C_0(z)$ represents the fog water generation rate ($\mathrm{g}\,kg^{-1}s^{-1}$) by cooling. The slope $\beta(p,T)$ can be expressed using the Clausius-Clapeyron equation,

$$\beta(p,T)=\frac{622L_v e_s(T)}{R_v T^2 p}, \tag{2}$$

where L_v and R_v, are the latent heat and the gas constant for vapor, respectively, and e_s is the saturation vapor pressure, computed with WMO recommended formulation (2008). *W(0)=0* and $W(H_{sat})=0$ are two boundary conditions for the ODE (1). Since in case of radiation fog, K is usually small and can be considered as a constant inside fog, the ODE (1) falls in the application scope of singular perturbation or asymptotic solution technique (Van Dyke 1964). According to ZF08, under a uniform cooling rate condition, the asymptotic solution of ODE(1) is

$$W(z,k)=[\frac{\beta(p,T)C_o H_{sat}}{\alpha}]^{1/2}[(1-\frac{z}{H_{sat}})^{1/2}-\frac{2}{1+e^{z/\delta}}], \tag{3}$$

where δ can be thought as a *fog boundary layer* (*FBL*), expressed as

$$\delta=\frac{K}{2[\alpha\beta(p,T)C_o H_{sat}]^{1/2}}, \tag{4}$$

The asymptotic solution Eq. (3) has one order of accuracy in terms of K, or O(K). In other words, the smaller the K is, the more accurate Eq. (3) will be. Since the turbulence intensity in a shallow fog is usually much weaker than that in a dense fog, Eq.(3) is more accurate for shallow fog than for deep fog.

The parameter δ represents the characteristic depth of turbulence mixing in liquid phase (in contrast to the mixing layer in the gas phase represented by a temperature profile) which is proportional to the turbulence strength and reversely to cooling rate and fog depth. Eq. (3) illustrates that a stable fog *LWC* vertical distribution is determined by a balance among three factors: cooling rate inside the fog, a positive values means continuously generate liquid water droplets to maintain the steady fog bank, gravitational settlement of the fog droplets, which

acts as an adjustor to redistribute newly generated liquid water from upper parts to lower parts of the fog, and turbulence effect. Because of negative sign of turbulence term (i.e. the δ term) in Eq. (3), turbulence always consumes the generated water inside the fog bank. Therefore, to persist a stable fog bank, these three effects must be in continuous balance. In other words, the droplets loss caused by gravitational settlement and turbulent diffusion must be offset sufficiently by a continuous generation of fog droplets by cooling. ZF08 suggested that the impact of turbulence on the fog bank can be expressed by the depth of *FBL* or value of δ. If the depth of the *FBL* is lower than the fog depth, or $\delta << H$, the fog can keep stable. Otherwise if $\delta \rightarrow H_{sat}$ or the *FBL* depth lifts upwards and reaches fog top (meaning turbulence influence is dominant in entire fog bank), fog will not be stable and be dispersed soon.

From Eq. (3) and δ, ZF08 found that the balance condition of fog bank can also be expressed by another parameter, so-called *critical turbulent exchange coefficient* K_c as shown below

$$K < K_c = 1.38[\alpha\beta(p,T)C_o]^{1/2} H_{sat}^{3/2} \quad . \qquad (5)$$

Eq. (5) says, to keep the balance in a steady fog, the turbulence intensity in the fog must be less than the critical turbulent exchange coefficients K_c, which is more sensitive to the fog depth ($H_{sat}^{3/2}$) than to the cooling rate ($C_o^{1/2}$). The critical turbulent exchange coefficient in (5) defines the upper bound of turbulence intensity which a persisting fog can withstand. An initial ground fog usually forms below 10 m near the surface and remains stable for a long time (conditioning) if the surface turbulence does not exceed the critical turbulent exchange coefficient K_c, otherwise the ground fog will dissipate. $K_c \sim H_{sat}^{3/2}$ means that a deep fog can withstand a much stronger turbulence without being dispersed than a shallow fog. That is why turbulence development is usually observed in a deep fog without dispersing but promoting the fog layer. Several factors may cause the turbulence intensity to exceed K_c: (1) a reduction in cooling rate (K_c decreases) due to sunrise, or local clouds, or warm advection; and (2) rising local wind speeds, which increase the surface mechanical turbulence (K increases). On the contrary, an increase in cooling rate or cessation of winds is in favor of persistence of ground fog.

2.2 Case with advection

It should be noticed that ODE (1) and its asymptotic solution Eq.(3) are for radiation fog without considering advection process. In case of other types of fog, advection may not be ignored. The steady fog *LWC* equation with advection can be expressed as following ODE

$$\begin{aligned} &K\frac{d^2W}{dz^2}+2\alpha W\frac{dW}{dz}+\beta(T,p)C_o(z)+Adv=0, \\ &W(0)=0, W(H_{sat})=0, \end{aligned} \tag{6}$$

where $Adv=-\vec{V}\cdot\nabla W$ is the *LWC* generation/reduction rate by horizontal moisture advection ($\mathrm{g}\,kg^{-1}s^{-1}$) and $\vec{V}$ is the horizontal wind vector within a fog bank. Given that *Adv* be a constant source or sink of liquid water content similar to the cooling rate in context of 1D fog, integration of ODE (6) following the same singular perturbation procedure as that in ZF08 yields

$$W(z,k)=\{\frac{[Adv+\beta(p,T)C_o]H_{sat}}{\alpha}\}^{1/2}[(1-\frac{z}{H_{sat}})^{1/2}-\frac{2}{1+e^{z/\delta}}], \tag{7}$$

where the *FBL* is expressed as

$$\delta=\frac{K}{2\{\alpha[Avd+\beta(p,T)C_o]H_{sat}\}^{1/2}}, \tag{8}$$

and balance condition becomes

$$K<K_c=1.38\{\alpha[Adv+\beta(p,T)C_o]\}^{1/2}H_{sat}^{3/2}. \tag{9}$$

The term inside the first [ ] in Eq. 9 is the total liquid water generation rate by both cooling and moisture advection. A positive *Adv* ($-\vec{V}\cdot\nabla W>0$) means a wet advection from upwind

brings more moisture into fog layer, leading to an increase in fog *LWC* while a negative *Adv* means a dry advection from upwind brings dry air into fog, leading to a decrease in fog *LWC*. Eq. (7) correctly reflects such an impact. If the dry air brought by upwind exceeds the amount of water droplets generated by cooling, the fog layer will disperse at all levels. The following fog *LWC* diagnostic scheme is designed based on Eq. (7) in attempt to deal with various types of fog. Moreover, Eq. (9) indicates that a wet advection strengths the critical turbulent exchange coefficient. As a result, fog is more difficult to be dispersed in a wet advection environment, which has been often observed in many long-lasting advection fog events.

3. Computation steps

3.1 input dataset

The vertical levels of model output data in a post processor can be either standard pressure levels or sigma levels. In general case, don't distinguish these two vertical level systems. Just assume the model data levels as its geographic height *Z*. Considering a general situation where terrain is not flat but has certain height H_{sfc}, the input data require following model output dataset:

(i) Vertical fields

(1) Geographic heights *Z(k)*, k=1,2,3, … above the sea level pressure with *k=1*

(2) Temperature *T(Z)*

(3) *RH(Z)*

(4) Wind speeds *WS(Z)*, or *u* and *v* components

(ii) Surface fields

(1) Surface height H_{sfc}

(2) 2m temperature T_{2m}

(3) 2m relative humidity RH_{2m}

(4) 10m wind speeds WS_{10m} , or u an v components at 10m

(5) 2m specific humidity, or relative humidity RH_{2m}

(iii) Cloud base H_{cloud_base} and cloud top H_{cloud_top}, both are above ground as reference.
If use sea level as reference, subtract the surface height H_{sfc} from them.

(iv)T_{2m} and $T(Z)$ in previous time step (to compute cooling rate)

3.2 Moisture advection computation

The *Adv* term is computed from wind and upwind total moisture, Q, which is equal to W + q, where W in $g\,kg^{-1}$, is fog liquid water content and q, also in $g\,kg^{-1}$, is specific humidity. Before conducting the fog *LWC* computation in a grid point, *Adv* should be calculated in advance using upwind wind speeds in x (component u) and y direction (component v) and total moisture. For simplicity, surface wind is used in *Adv* computation. Suppose the interested grid point is at (i,j), where i and j are grid index in x and y directions, respectively. The *Adv* in grid point (i,j) is computed according to following 4 upwind directions as shown in Fig. 1:

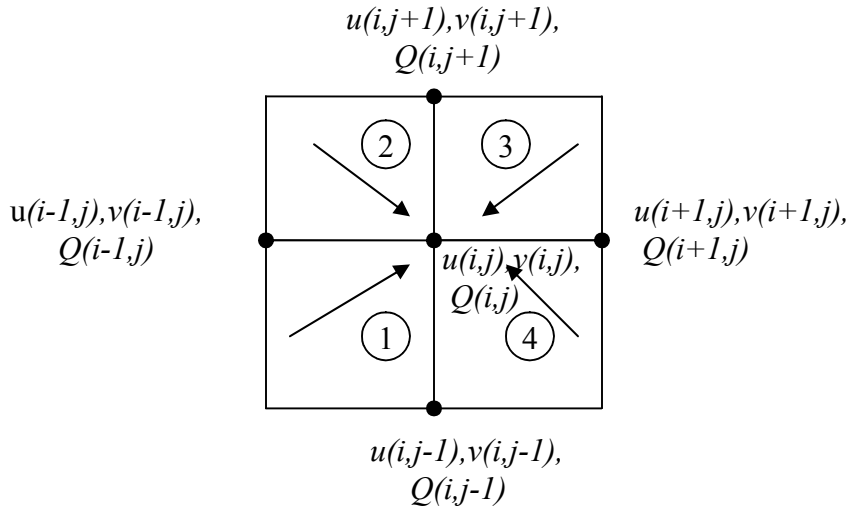

Figure 1. Moist advection cases according to 4 wind directions

Case 1: if $u(i,j) \geq 0$ *and* $v(i,j) \geq 0$

$$Adv = -u(i,j)*[Q(i,j)-Q(i-1,j)]/dx - v(i,j)*[Q(i,j)-Q(i,j-1)]/dy\ , \qquad (10.1)$$

Case 2: if $u(i,j) > 0$ and $v(i,j) < 0$

$$Adv = -u(i,j)*[Q(i,j)-Q(i-1,j)]/dx - v(i,j)*[Q(i,j+1)-Q(i,j)]/dy \quad (10.2)$$

Case 3: if $u(i,j) < 0$ and $v(i,j) < 0$

$$Adv = -u(i,j)*[Q(i+1,j)-Q(i,j)]/dx - v(i,j)*[Q(i,j+1)-Q(i,j)]/dy \quad (10.3)$$

Case 4: if $u(i,j) < 0$ and $v(i,j) > 0$

$$Adv = -u(i,j)*[Q(i+1,j)-Q(i,j)]/dx - v(i,j)*[Q(i,j)-Q(i,j-1)]/dy \quad (10.4)$$

where u and v are surface wind components (at 10m) in x and y directions, dx and dy are grid space in x and y direction, respectively. The above 4 cases ensure when upwind grid is more moist than present grid, the Adv is wet advection ($Adv>0$), otherwise it is dry advection ($Adv<0$).

3.3 Turbulent exchange coefficient computation

If there is no direct turbulent exchange coefficient K output in a model post processor, nor turbulent kinetic energy either, the required turbulent exchange coefficient K can be estimated from classic M-O similarity method. That is, calculation of K is based on Richardson number Ri, which is estimated from both vertical gradients of temperature and wind speeds. In the classic M-O similarity method, a stability parameter S is first estimated from Ri, then the K can be further computed from the stability parameter. There are several formulations to compute stability parameter S. But in operational models, for some practical reasons, 'long tail' format of S is used. That is that Ri may overpass its critical value (0.25) when the air is extreme stable and turbulence tends to cease ("long tail" dash line for $Ri \sim S$ relationship as shown in a conceptual plot in Fig 2). When $Ri > 0.25$, the "long tail" form of turbulence computation in an operational model is prone to over-estimate turbulence intensity (Beare, et al. 2006). Thus

for fog diagnosis in a post processor, the 'short tail' format (the solid line as shown in Fig. 2) should be resumed.

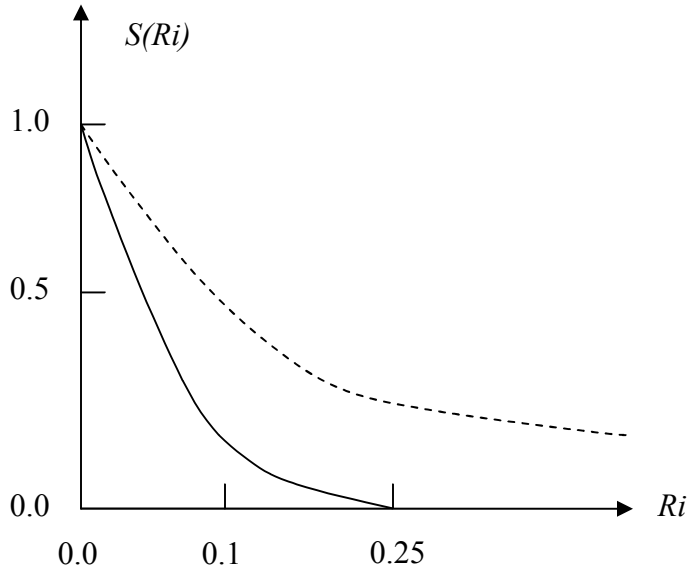

. **Figure 2**. Long tail and sharp tail curves of $Ri \sim S$ (stability function) in stable condition

In order to constrain the turbulence as $Ri > 0.25$, a sharp curve for $Ri \sim S$ relationship is used (solid line in Fig. 2). Thus following method is applied depends on the sign of Ri computed from model temperature and wind speed profiles:

$$Ri = \frac{9.8}{\overline{T}} \frac{[(T(Z_T) - T_{2m})/(H_{sat} - 2) + 0.01]}{[(WS(Z_T) - WS_{10m})/(H_{sat} - 10)]^2}, \qquad (11.1)$$

where $\overline{T}$ is average temperature computed from $0.5*[T(Z_T) + T_{2m}]$, Z_T the fog top or saturated layer height, and H_{sat} the fog depth (i.e. saturated layer depth). Before this computation, the saturation depth should be first searched from vertical level RH data as shown in Fig. 4.

If Ri ≤ 0, then (unstable case suggested by Beljaars 1992)

$$C_h = \frac{12(1 + H_{sat} / z_0)^{1/2}}{[\ln(1 + H_{sat} / z_0]^2}$$
$$S(Ri) = 1 - \frac{10Ri}{1 + C_h(-Ri)^{1/2}} \quad , \qquad (11.2)$$

while if ($Ri > 0$, sharp format suggested by Beare et al. 2006)

$$S(Ri) = (1 - 5Ri)^2 \quad \text{for } 0 < Ri < 0.1, \qquad (11.3)$$

$$S(Ri) = (1/20Ri)^2 \quad \text{for } Ri \geq 0.1, \qquad (11.4)$$

where z_0 is roughness length (0.02 m is assumed). It can be tested that when Ri is over 0.25, the stability parameter S becomes very small.

After the stability parameter $S(Ri)$ is estimated, the turbulent exchange coefficient K can be calculated from following equation (Bears et al. 2006)

$$K = \lambda^2 \left| \frac{WS(Z_T) - WS_{10m}}{H_{sat} - 10} \right| S(Ri), \qquad (12)$$

where λ is mixing length, defined as (Beare et al. 2006):

$$\frac{1}{\lambda} = \frac{1}{0.4(H_{sat} + z_0)} + 0.025 \qquad (13)$$

3.4 LWC computation

The scheme computation is divided into 2 situations. First case is for clear sky case. In this case, no low stratus cloud exists and H_{sat} is searched upward from the ground. The second case is for low stratus cloud. In this case, the fog depth is defined as the depth of the stratus cloud.

3.4.1 Clear sky case

Step 1. Select a saturation threshold RHs

Different model has a different saturation threshold *RHs*, usually ranging from 90 to 100 %, depending on model bias. Thus, for a dry biased model, even when *RH* is less than 100% at a grid point, fog still can be diagnosed there as long as the relative humidity threshold *RHs* is set to a value smaller than 100%.

In case of extreme low temperature (e.g. < -20 ^{o}C), ice fog may happen. In freezing condition, the saturation threshold *RHs* over ice can be determined by e_i/e_s, where e_i and e_s are saturation vapor pressures over ice and over liquid water, respectively. Here the WMO 2008 recommended formulations are used:

$$e_i = 6.112\exp[22.46T(272.62+T)], \quad \text{and} \tag{14.1}$$

$$e_s = 6.112\exp[17.62T(243.12+T)], \tag{14.2}$$

where T is temperature in ^{o}C. In very low temperature, saturation threshold *RHs* over ice may be much smaller than that over liquid water. For example, the air of *RH* with reference to (w.r.t.) water ~ 70% will be saturated w.r.t ice if temperature is below – 40 ^{o}C. The saturation threshold *RH*s w.r.t. ice under very low temperature can be determined by the ratio of e_i/e_s. The ratio in different low temperature is shown in Fig. 3

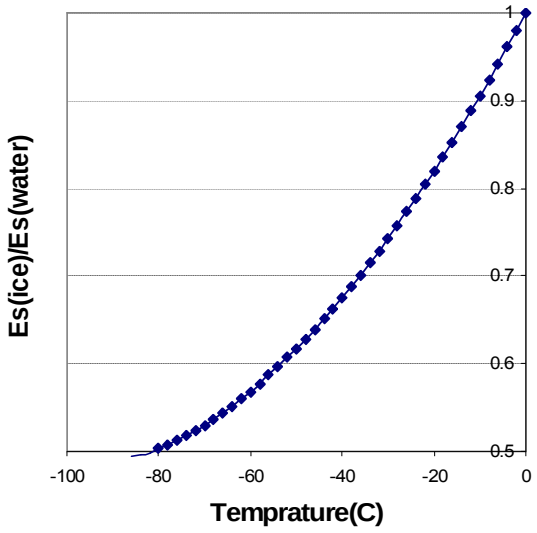

Figure 3. Ratio of e_i to e_s under different temperature below 0 ^{o}C

It is observed that the lower the temperature, the lower the saturation threshold *RHs* will be. At −80 ^{o}C, this ratio is only 0.50. In other words, *RHs* reaches as low as ~ 50% , ice fog can form.

Step 2. Search saturated layer depth from ground

With selected saturation threshold *RHs,* the saturated levels are searched, one level by one level, upward from the surface (2m). There are three cases for this search: case 1, no saturated level is found. In this case, no fog likely forms. The scheme retunes 0 *LWC*; case 2, only 2m level is saturated and all other levels above are not saturated. In this case, very thin saturated layer is diagnosed and its depth, H_{sat}, is set to 2m; case 3, more levels in addition to 2 m level are found to be saturated. In this case, the depth of the highest saturated level, Z_T , is set to be the saturated layer depth H_{sat}. If the model level is based on sea level, surface height should be subtracted from Z_T. That is $H_{sat} = Z_T - H_{sfc}$. See Fig. 4 where saturation threshold *RHs* is set to 100%.

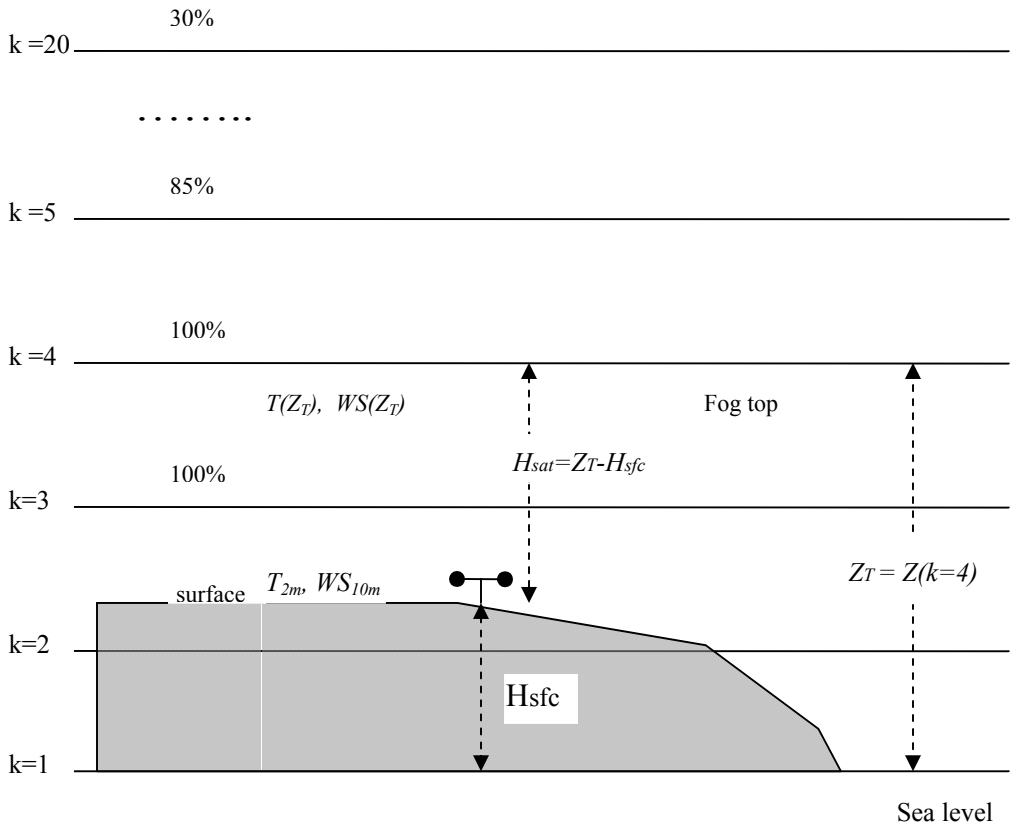

Figure 4. Fog depth is searched vertically with *RH* threshold *RHt*~100%

After a surface saturated layer is found, wind speed shear and temperature vertical gradient can be computed from wind speeds and temperature at both Z_T and 2 m levels. In case of 2 m saturated layer, temperature and wind speeds at 2m and at the level just above 2m are used to calculate *Ri*. The stability parameter and turbulent exchange coefficient within the saturated layer can be computed with Eqs. 11-13. Readers are reminded that a saturated layer does not necessarily mean existence (occurrence and persistence) of a fog. As discussed in the previous sections, existence of a fog also depends on cooling rate and turbulence strength.

Step 3. Cooling rate computation

If a saturated layer is found near the surface, the next thing is to see if a cooling process happens within the saturated layer. The cooling rate is computed from current and previous time's temperature profiles. If the saturated layer depth is only 2m, the cooling rate is computed with $C_o = [T_{2m}(n)-T_{2m}(n-1)]/\Delta t$, where $T_{2m}(n)$ and $T_{2m}(n-1)$ are present and previous

time step's 2m temperature, and Δt is time step (in sec). If the saturated layer depth is higher than 2m, the cooling rate is an average of the cooling rates at the saturated layer top and 2m, that is $C_o = 0.5*\{[T(Z_T,n)-T(Z_T,n-1)]/\Delta t + [T_{2m}(n)-T_{2m}(n-1)]/\Delta t\}$, where $T(Z_T,n)$ and $T(Z_T,n-1)$ are temperature at the saturated layer top (Z_T) in current and previous time, respectively.

Step 4. Total LWC generation

The total fog *LWC* increment or decrement due to cooling/warming and wet/dry advection is computed from

$$C\_Adv = \beta(\overline{T}, p)\cdot C_0 + Avd\ , \qquad (15)$$

where $\overline{T}$ is average temperature computed from 0.5*[$T(Z_T,n)$ and $T_{2m}(n)$], p the surface pressure. If $C\_Adv < 0$, the saturated layer is in vaporization stage caused by dry advection, or warming, or dry advection exceeding the amount of water droplets by cooling. In this case, the computation is stopped and 0 is returned to *LWC*.

Step 5. Maximum LWC in the fog layer

If $C\_Adv > 0$, the maximum value for the asymptotic *LWC* profile can be computed from

$$W_{\max} = \left[\frac{C\_Adv\cdot H_{sat}}{\alpha}\right]^{1/2}\ . \qquad (16)$$

Step 6. Vertical LWC distribution

With the maximum *LWC* (16) and the *FBL* value δ computed from Eq. (8), the *LWC* profile inside the saturated layer is computed from:

$$W(z) = W_{\max}\cdot[(1-\frac{z}{H_{sat}})^{1/2} - \frac{2}{1+e^{z/\delta}}], \qquad (17)$$
$$0 \le z \le H_{sat}$$

If $W(z) < 0$ (this implies that $K>K_c$), then set $W(z) = 0$ at all levels and return. Otherwise, it means that the saturated layer is fog layer filled with liquid water droplets. The surface *LWC* is set to *W* at z =10m.

In above computation steps, the fog persistence condition $K<K_c$ is not pursued. However, if $W(z)$ at any level is larger than 0, the fog persistence condition will automatically satisfied. To make sure for this, the K_c can be computed as follows

$$K_c = 1.38 \times 0.062 \times C\_Adv \times H_{sat}^{3/2} \qquad (18)$$

3.4.2 Low stratus cloud case

In case of appearance of low cloud stratus with cloud top < 400 m and cloud base < 50 m (the first model level above the ground), the first 2 computation steps will give rise to following 2 steps. This implies that the model output cloud has a higher priority than the clear sky procedure. In other words, if model has a surface cloud at a grind point, the scheme recognizes it as a fog without searching saturated level. Just set the fog depth as cloud depth. It is noted that the cloud top and base heights in the models at NCEP are defined as the vertical location where the cloud *LWC* threshold ~ 10^{-3} gkg^{-1}, a vlaue much smaller than the fog *LWC* threshold 0.016 gkg^{-1} (equivalent to visibility ~ 1000 m). Therefore, the surface cloud (fog) *LWC* must be computed from this scheme to adjust the model *LWC* at the surface in this case.

Step 1. Determine if the cloud is low stratus that touches down the ground.

If H_{cloud_top} < 400 m and H_{cloud_base} < 50 m at same time, the cloud is considered as a surface fog. Then set fog depth H_{sat} to be H_{cloud_top} (see Fig. 5).

Step 2. Search the level just below the cloud top

The method is searching from the cloud top H_{cloud_top} downward to find the level just below the fog top. Set this level as Z_T.

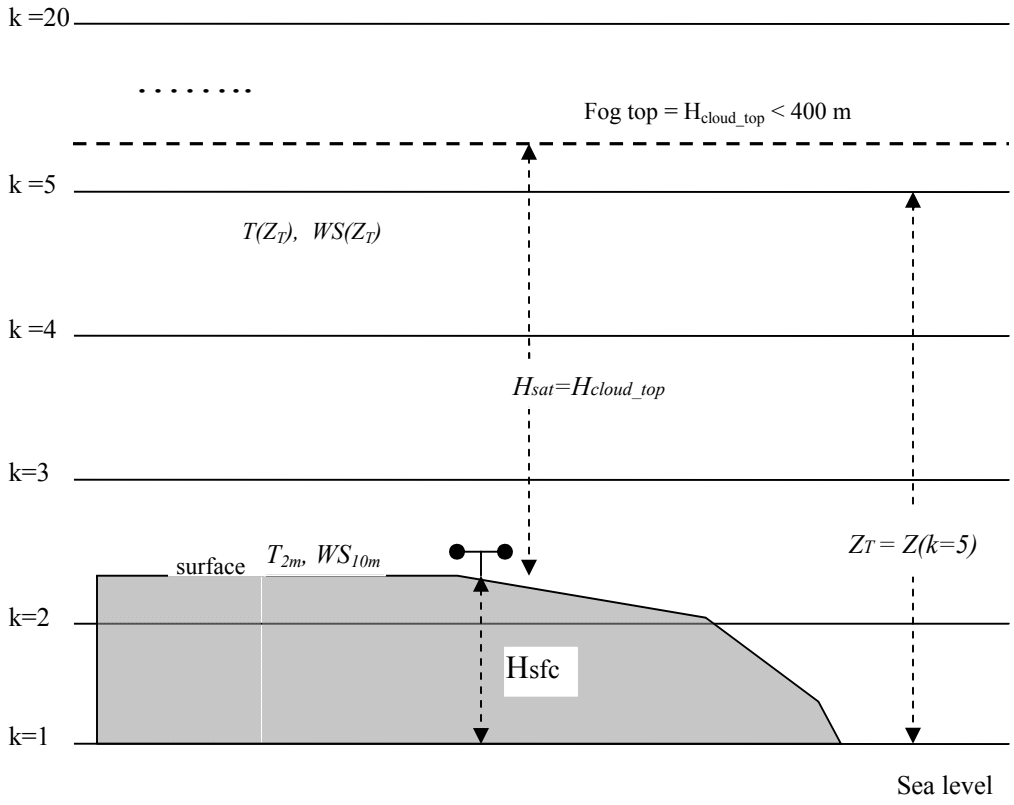

Figure 5. Low stratus that touchdowns is considered as fog

After Z_T is found, we will repeat Step 3 in section *4.3.1* for computing the *LWC* in the low stratus. The entire procedures are summarized in Fig. 6.

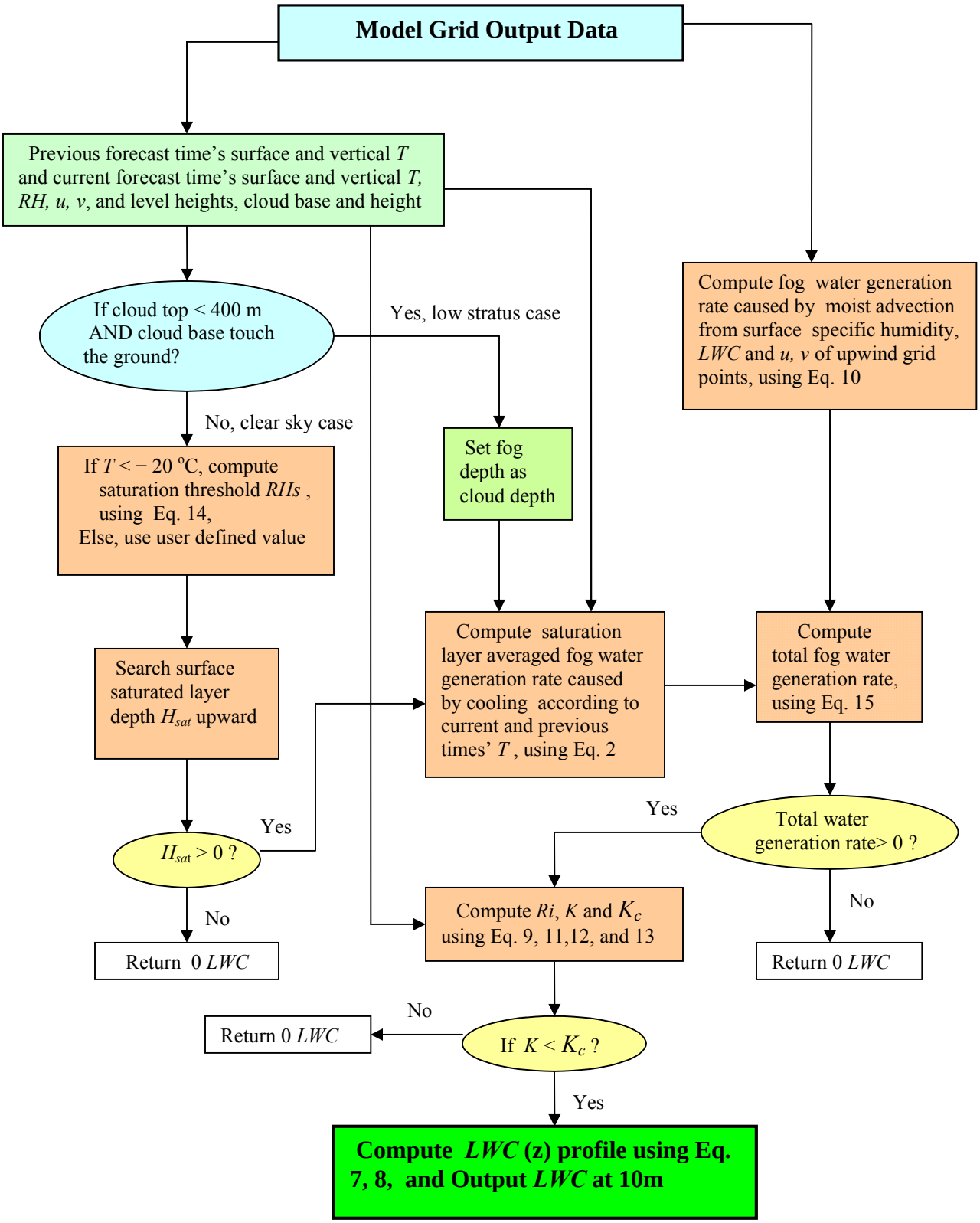

Fig. 6, Fog diagnostic scheme flowchart

4. Discussion on accuracy and uncertainties

Errors and uncertainties of the asymptotic *LWC* formulation Eq. (3) or Eq. (7)have been discussed in detail by Zhou and Ferrier (2008) from six different aspects. They are summarized as follows.

(1) It is an asymptotic solution with a truncation error of *O(K)*. This means that the solution is more accurate for a small *K* than for a large *K*. The accuracy of the asymptotic solution for different *K* values can be evaluated by comparing the asymptotic solution with the numerical solutions of ODE (1) in different *K* values as presented in Fig. 7. We can seethat the *LWC* profiles for the asymptotic and the numerical solutions are in a close agreement with a small positive bias of 10 % for weak turbulence (Fig. 7a for shallow fog and 6d for deep fog) and a larger positive bias of 30 % for strong turbulence (Fig. 7b for shallow fog and 7*e* for deep fog). However, if the turbulence intensity further increases, being close to K_c, both asymptotic and numerical *LWC* approach zero (Fig. 7c and 7f).

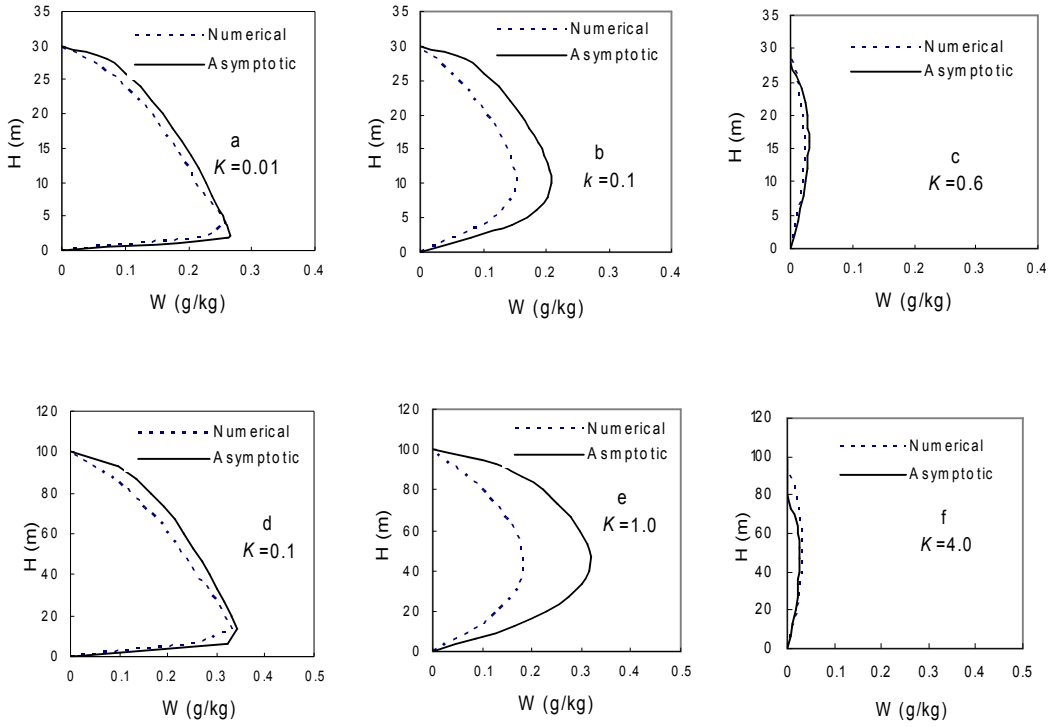

Figure. 7. Comparisons between numerical and asymptotic solutions of Eq. (1) for different turbulence exchange coefficients (in $m^2 s^{-1}$) and fog depths: (a)-(c) H_{sat} = 30 *m*, and (d)-(f) H_{sat} = 100 *m*. α = 0.062, T = 0.0 ^oC, cooling rate = 1.0 $^oC\ hr^{-1}$ for the all cases.

(2) The asymptotic solution is derived under steady condition of fog, which is not always held in fast developing or dissipation stages of fog. However it should be kept in mind that any diagnosis in a model post is always under the assumption of steady or quasi-steady phase of variables, implying that a diagnosed variable in a model post processor represents its average status over a period of time. So, the fog *LWC* distribution is not instantaneous value but an average over a period from previous to current output time (usually 1 hour of interval time for NCEP models).

(3) The asymptotic formulation also requires a vertically-uniform *K* as an input parameter. But in fog, *K* varies with heights. To evaluate the impact of the uniform *K* assumption on the asymptotic solution, particularly in a deep fog, two numerical solutions of ODE (1) for an 100 m fog are compared in Fig. 8, one with *K* linearly increasing from zero at the surface to a maximum value of 1.0 $m^2 s^{-1}$ at 70 m and then linearly decreasing to zero at the fog top, another one with a uniform value of 0.5 $m^2 s^{-1}$, representing the average of the first case. Fig. 8 shows that the two *LWC* profiles are not significantly different. So the uniform *K* assumption is not, at least in terms of solution accuracy, a serious problem when the solution is applied to deep fog.

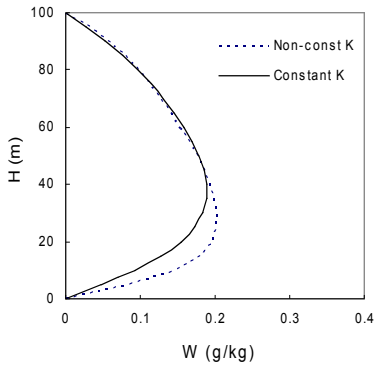

Figure 8. Numerical solutions of ODE (1) for linearly-distributed *K* with maximum 1.0 $m^2 s^{-1}$ at 70 m (dash) and uniform *K* with a constant value 0.5 $m^2 s^{-1}$ (solid). H_{sat} =100 *m*, α = 0.062, *T* = 0.0 ^oC, cooling rate = 1.0 $^oC\ hr^{-1}$ for both cases

(4) It can be expected that how to compute K has an impact on the result since it directly affects the balance condition of fog at a grid. In ZF08, three classic methods were applied to examine the impact of turbulence computation on the persistence conditions, including the formulation of Businger et al. (1971), the improved formulation of Duynkerke (1991), and the level-2 formulation of Mellor and Yamada (1974). The results show a quite large difference among these methods although the general trend is similar, particularly during the fog formation stage when the surface is extremely stable. In current version of this scheme, to speed up computation, the parameter Richardson number Ri is first estimated and then compute the stability parameter to obtain the turbulent exchange coefficient. It is noted that there are several parameters for the stability parameter expressions (Beare et al. 2006), these parameters can also be tuned depending on applications. Since the asymptotic formulation is more accurate for shallow fog, using K_c is more suitable for diagnosis of a stable shallow fog or a fog during its formation than for diagnosis of its dissipation. The verification of K_c by Zhao et al. 2010 using observational fog data has also proved this suggestion.

(5) Cooling rate is assumed as a constant value which represents an average cooling within a fog bank. In real world inside fog, it is not constant but varies with height, particularly in deep fog, in which cooling is generally reaches its maximum near the fog top and then reduces downward until it become warming near the ground. Using a linear distribution of cooling rate along vertical direction with a real fog data in New York, ZF08 compared its result with a constant cooling rate and found that there is no big difference in resultant LWC distributions between these two cooling rates, particularly near the ground.

(6) The constant α is introduced to parameterize the droplet gravitational settling velocity in fog. It is assumed to be 0.062 as suggested by Brown et al. (1976) based on several fog's field observations. In general situations, it may not be a constant for different types of fogs. However, based on the sensitivity experiment by ZF08, it is not so sensitive to the fog LWC around the value 0.062. For ice fog, α is still uncertain. For current scheme, value for liquid water is still used for ice fog. But some observation suggested that it falls in same range as liquid droplets.

5. Testing examples

In this section, some examples of model output data (surface and vertical data) are used as input for testing this scheme. The number of surface levels is 14, from 50m above the ground up to 2900 m. All of following examples have same grid space $dx = dy \sim 10$ km, and same time step interval 3600 seconds.

5.1 Clear sky without advection

This is a radiation fog case. The input data at 14 levels and the surface are listed in Table 1. Set *RH*s=95% as saturation threshold. Other input data: $H_{cloud\_top} = 20$ km, $H_{cloud\_base} = 20$ km, (in NCEP models, a large value for cloud top and base means that there is no cloud) and $Adv = 0$. t_1 and t_2 are model's previous and current output times.

Table 1. Vertical and surface input data

Levels	***Z* , m**	***T*(t$_1$), ^{o}C**	***T* (t$_2$), ^{o}C**	***u*(t$_2$), m/s**	***v*(t$_2$), m/s**	***RH*(t$_2$),%**
14	2900	-6.4	-6.4	9.9	1.5	20.6
13	2600	-5.2	-5.2	9.8	2.9	24.1
12	2300	-4.9	-4.9	9.6	6.7	30.7
11	2000	-3.4	-3.4	9.6	4.6	31.5
10	1600	-2.5	-2.5	9.4	5.4	32.1
9	1300	-1.2	-1.2	9.4	6.9	32.0
8	1000	-0.9	-0.9	8.3	6.6	33.5
7	800	3.3	3.3	7.2	5.0	33.0
6	600	4.7	4.7	6.1	5.5	44.0
5	450	5.4	5.4	5.2	4.4	51.3
4	300	6.5	6.0	4.2	4.2	60.2
3	200	6.8	6.5	3.5	3.4	83.5
2	100	7.5	7.0	3.0	3.8	97.3
1	50	7.1	6.8	1.8	2.3	97.1
Surface	***Z*, m**	***T*$_{2m}$(t$_1$), ^{o}C**	***T*$_{2m}$(t$_2$), ^{o}C**	***u*$_{10m}$(t$_2$), m/s**	***v*$_{10m}$(t$_2$), m/s**	***RH*$_{2m}$(t$_2$),%**
	30	6.7	5.5	1.0	1.2	97.5

With *RHs* = 95% as saturation threshold, searching the saturated levels upward from the surface will find $Z_T = 100$ m. Thus the saturated layer depth $H_{sat} = Z_T - H_{sfc} = 100 - 30 = 70$ m. The averaged cooling rate is 0.000236 $^oCs^{-1}$, or 0.85 $^oChr^{-1}$, equivalent to water generation rate

of 0.385 $g/kg\,hr^{-1}$ With the temperature at 2m (above the ground) and 100 m (above the sea level), *Ri* can be computed form Eq. (11.1). The resultant *Ri* = 0.38. With this *Ri* value, the stability parameter *S* = 0.26, and *K*=0.26 $m^2 s^{-1}$. The *FBL* value δ =8.3 m, much lower than H_{sat}. So the fog can form and persist, which can be verified by K_c. In this case K_c = 1.53 $m^2 s^{-1}$, which is much larger than the value of *K* (0.26 $m^2 s^{-1}$). The *LWC* profile within the fog layer is divided to 10 levels. At each level the *LWC* is computed and presented in Table 2, showing that around 28 H_{sat} m the fog *LWC* reaches its maximum value

Table 2. Computed LWC within the 70m-depth fog bank

Z(m)	0	7	14	21	28	35	42	49	56	63	70
W(g/kg)	0	0.16	0.25	0.27	0.26	0.24	0.22	0.19	0.16	0.11	0

5.2 Clear sky with dry advection

Suppose all input data are same as previous case but has dry advection with $Adv \sim -0.00005$ g/kg s^{-1} or −0.180 g/kg hr^{-1}, which is still less than the cooling generation rate. So the total water generation is positive (0.385−0.180=0.205 *g/kg/hr*) and the resultant *LWC* is presented in Table 3, showing that the overall *LWC* at all levels is reduced. It can be tested that if the dry advection amount is tripled to −0.54 g/kg hr^{-1} (0.385−0.54 = −0.155 < 0), fog will be completely dispersed.

Table 3. Computed LWC within the 70m-depth fog bank with dry advection

Z(m)	0	7	14	21	28	35	42	49	56	63	70
W(g/kg)	0	0.08	0.15	0.18	0.18	0.17	0.16	0.14	0.11	0.08	0

5.3 Clear sky without advection but warming near the surface

Suppose all input data are same as the first case but 2m temperature increase from previous time 6.7 ^{o}C to current time 6.8 ^{o}C, then there will be no *LWC* on all levels with the saturated layer. In this case, K_c = 1.03 $m^2 s^{-1}$, while *K* = 1.61 $m^2 s^{-1}$, larger than K_c. *FBL* value δ = 75.5

m, which is also higher than the saturated layer depth 70m. Both indicates the fog layer is not stable so that no fog is there or it has been dispersed.

5.4 Low stratus with wet advection

Suppose cloud top is 200 m and cloud base is 40m, then this falls into low stratus category, and suppose there is wet advection $Adv \sim 0.00005$ g/kg sec^{-1}, then the *LWC* profile with the fog is shown in Table 4.

Table 4. Computed LWC within the 200 m-depth fog bank

Z(m)	0	20	40	60	80	100	120	140	160	180	200
W(g/kg)	0	0.67	0.63	0.59	0.55	0.50	0.44	0.39	0.31	0.22	0

6. A case study for warm fog in Gulf coast

Fig. 9 is METAR (Meteorological Aviation Report) surface data showing a series fog events that occurred on 23-24 November 2010 along the Gulf coast in Texas, Louisiana, Mississippi, and Florida. These heavy fog events caused several fatal accidents on highways in these states and a BP oil company airplane crash which killed 3 people including the BP's Gulf Oil-Spill Recovery chief commander, a Texas lawyer, and a pilot who attempted to land the airplane at the Destin Airport, Alabama, in a heavy fog condition. Fig. 10 is ADDS (Aviation Digital Database System of AWC, NCEP) visibility analysis data over entire Contiguous US (CONUS) on 23-24 November 2010, showing no other big fog event except one near smoky mountain. KY. This study only focuses on the Gulf coast fog case.

.

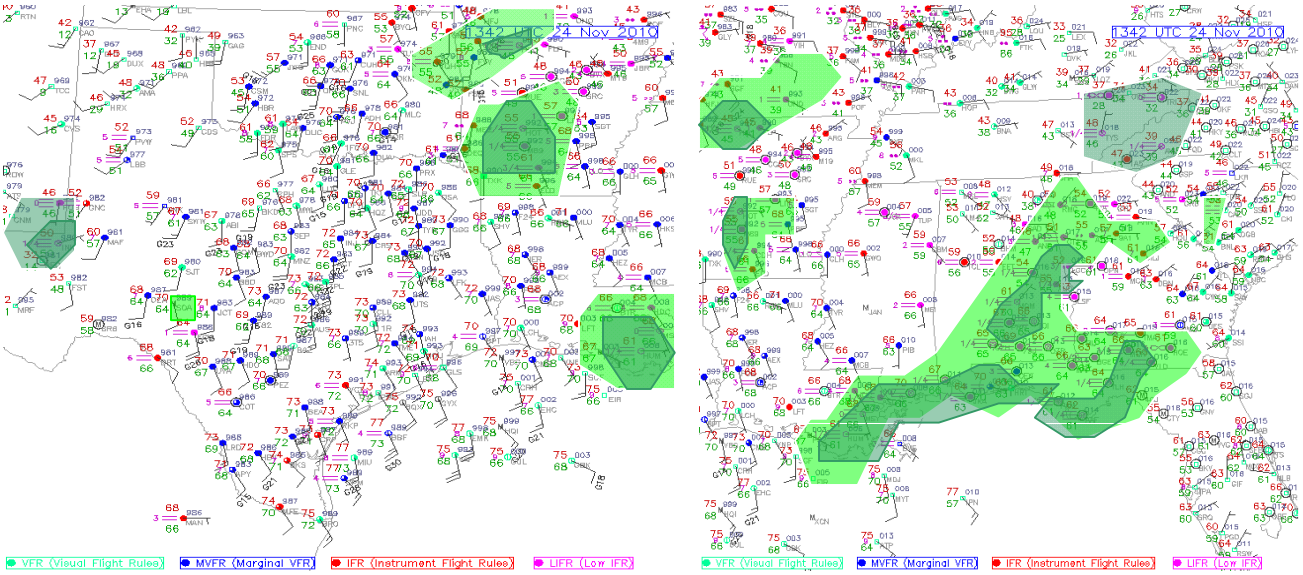

Fig. 9. METAR data over Texas (left) , Louisiana, Mississippi, and Florida (right) on 12Z (local time 06:00 am), 24 November 2010. Light green shade indicates fog with visibility < 1000 m (or ¾ mile), deep green indicates dense fog with visibility < 400 m (or ¼ mile).

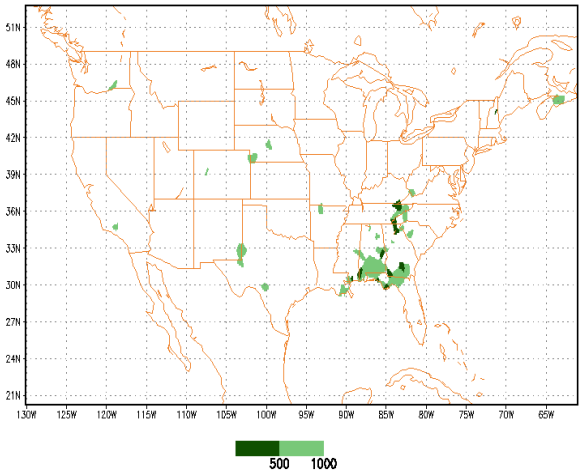

Fig. 10 ADDS visibility analysis data (m) over CONUS at 12Z, 24 November, 2010

Following are predictions for Nov 23-24 Gulf coast fog event, from ARW-WRF, RUC and VSREF, respectively, with the present scheme and compared with the results of the visibility and multi-rule methods from the same models.

6.1 32 km WRF-ARW

The 32 km resolution ARW-WRF model (NCAR-WRF) shown here is a base model of the NCEP Short Range Ensemble Forecast System (SREF). In Fig. 11, 9 hour forecast results from 32km ARW with 3 methods are presented for the Gulf coast fog event: visibility diagnosed, multi-rule diagnosed and new diagnostic method. Fig. 11 shows that the fog was totally missed by the visibility diagnosis, and the multi-rule diagnosis captured only a very small part of the fog event in Alabama coast while the present scheme predicted most part of the fog regions although there are some FAR in some other areas. Please also note that the present scheme not only predicted fog regions but also fog *LWC* (in g/kg) to show fog intensity.

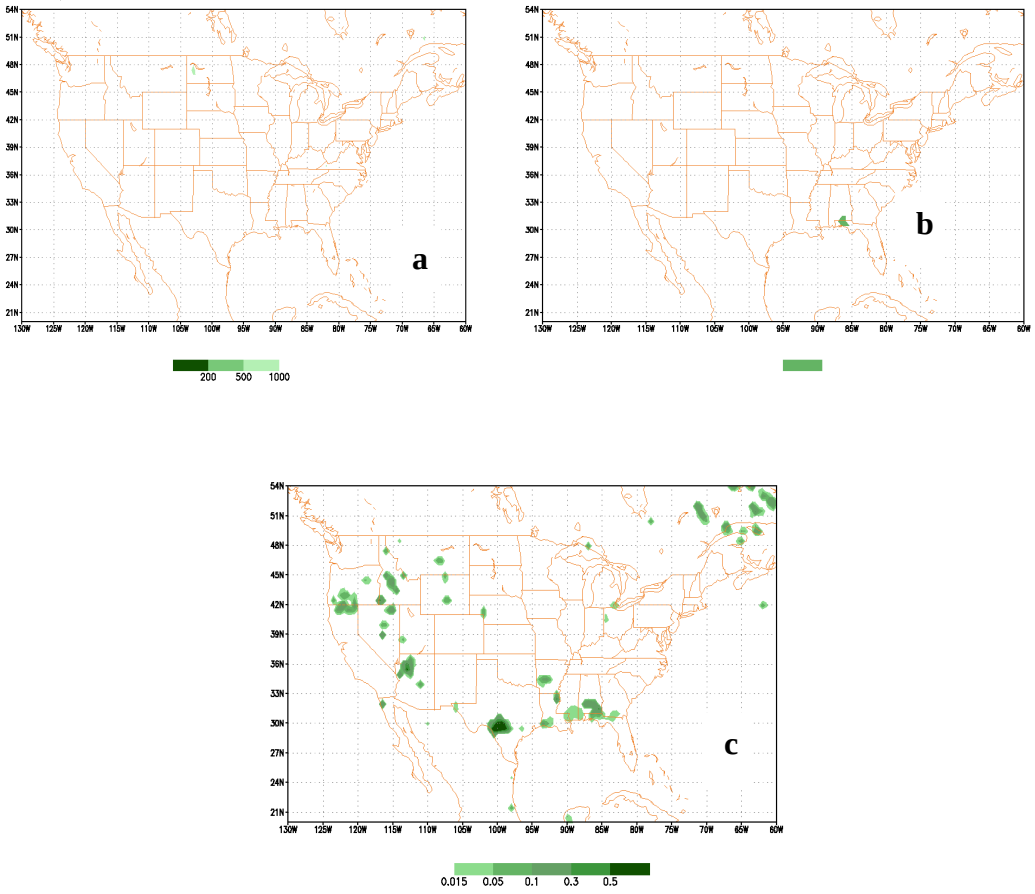

Fig. 11, 9 hour 32km-ARW fog predictions for Nov 23-24, 2010 regional fog events with visibility (m) detection (a), "yes" regions with multi-rule detection (b) and *LWC* (g/kg) with present scheme(c). The 32 km-ARW run at 03Z and validated at 12Z on Nov. 24, 2010.

6.2 13 km RUC

13 km resolution Rapid Update Cycle model (RUC) is a NCEP model specific for aviation weather prediction that runs hourly per day out to 18 forecast hours. Current operational RUC has visibility output that can be used to diagnose fog as shown in Fig. 12a. By diagnosing other output variables with multi-rule method, fog occurrence also can be predicted as shown in Fig. 12b. Comparing Fig. 12a and b, both methods created very similar regional fog forecasts. However, both forecast fog regions in Gulf coast are smaller that those shown in Fig. 10. With similar RUC output data by applying the present scheme, the fog *LWC* was predicted as shown in Fig. 12c, which shows larger fog regions than those diagnosed by visibility and multi-rule methods.

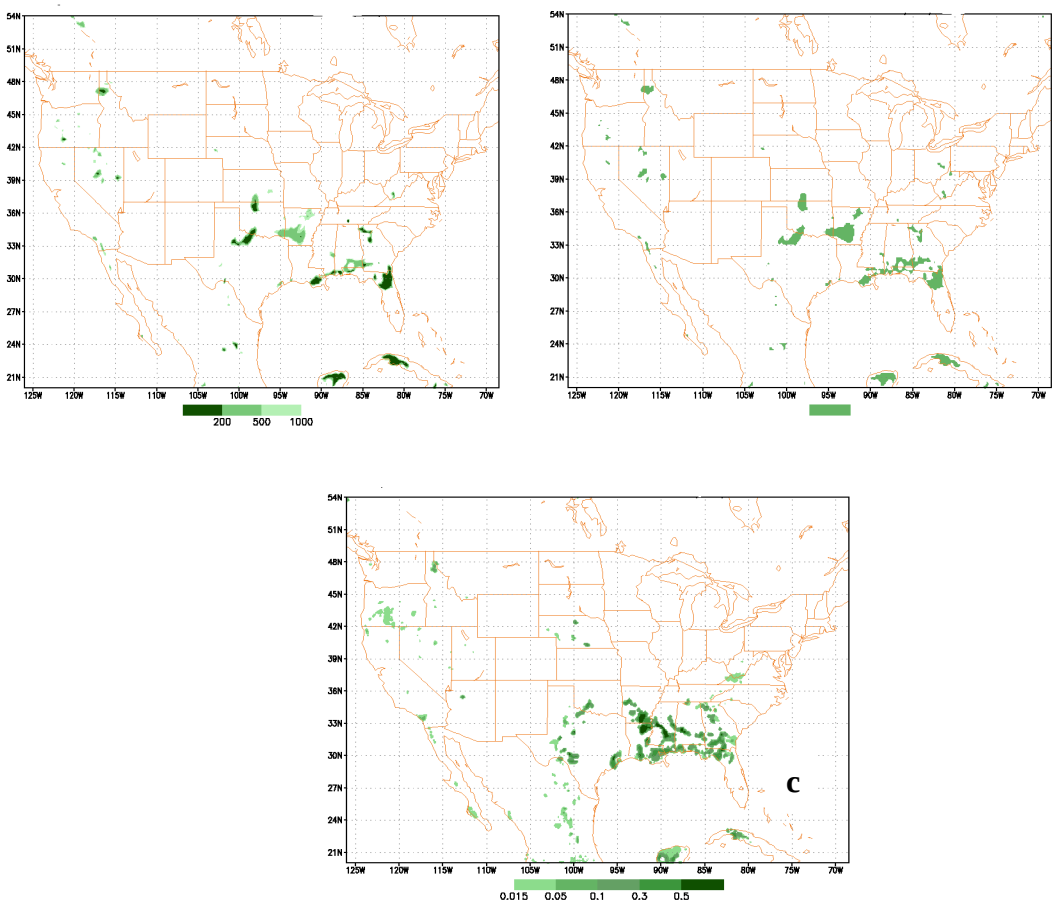

Fig. 12, 9 hour RUC fog predictions for Nov 23-24, 2010 regional fog events with visibility (m) detection (a), "yes" regions with multi-rule detection (b) and *LWC* (g/kg) with present method (c). The RUC run at 03Z and validated at 12Z on Nov. 24, 2010. 13 km RUC run at 03Z and validated at 12Z on Nov. 24, 2010.

6.3 VSREF

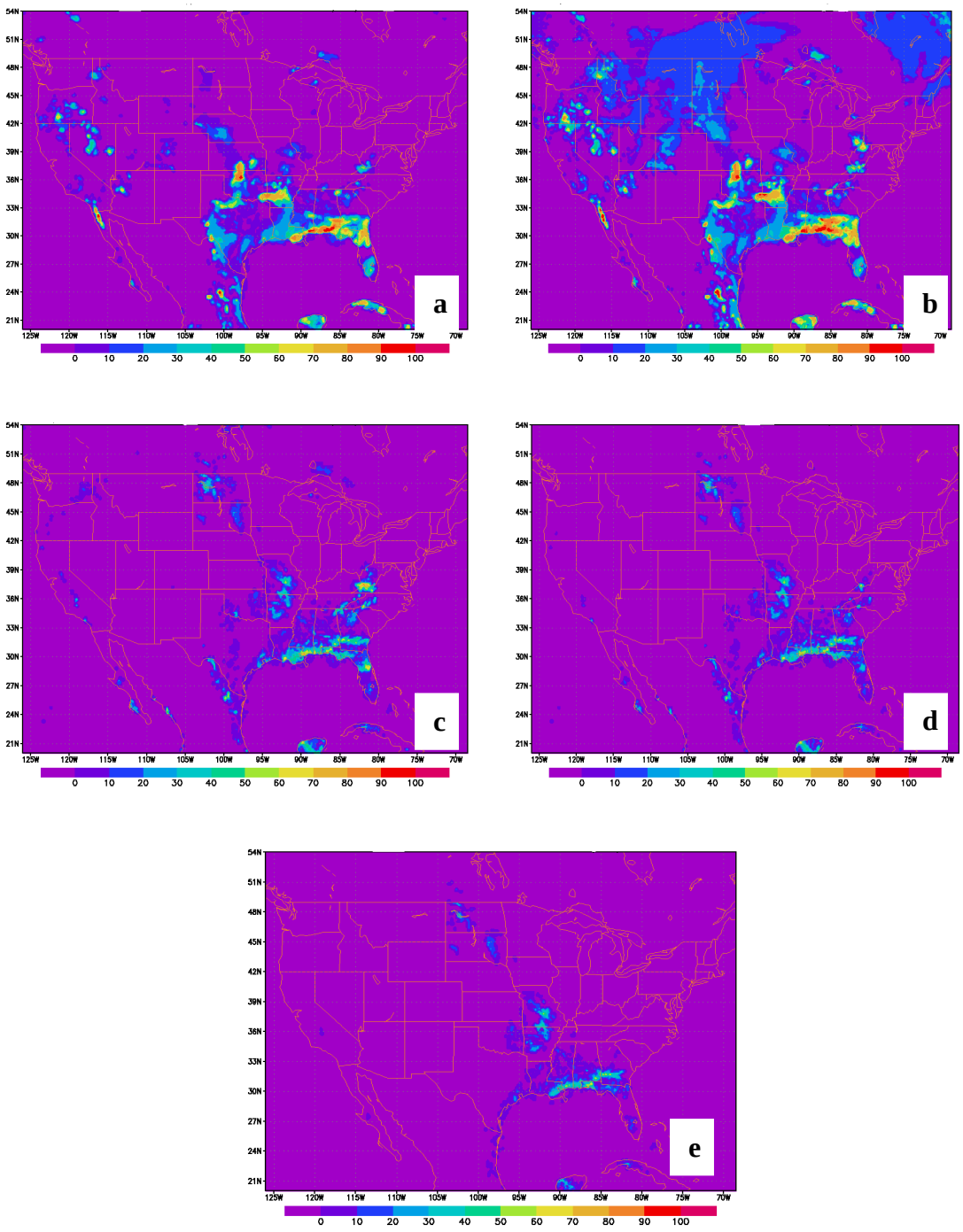

Fig. 13. 9 hour fog probabilistic predictions from VSREF with visibility < 1000m diagnosis method (a), multi-rule yes-no diagnosis method (b) and present scheme (c for fog probability with visibility < 1000 m, d for medium intensity fog probability with visibility < 500 m, and e for dense fog probability with visibility < 200m). The VSREF run at 03Z and validated at 12Z on Nov. 24, 2010.

The NCEP's Very Short Range Ensemble Forecast System (VSREF) was developed specifically for aviation weather ensemble forecast under FAA support, which is generated from NAM and RUC models with time lag technique. The visibility related probabilistic products in the VSREF include surface visibility probability by using visibility diagnosis, fog occurrence probability by using multi-rule diagnosis and fog intensity probability with the present method. For the present scheme, the grid-wide fog *LWC* is first diagnosed and then converted the *LWC* value to visibility range with Stoelinga and Warner (1999) method. See (http://www.emc.ncep.noaa.gov/mmb/SREF_avia/FCST/VSREF/web_site/html/fog.html). 9 hour fog probability forecasts with these three methods for Nov 23-24 Gulf coast fog event are displayed in Fig. 13a, b, c, d, and e, respectively. Comparing Fig. 13.a and b with Fig. 10, one can observe that the Nov. 23-23 Gulf coast fog regions are fully covered by both visibility and multi-rule generated fog probabilities if using "probability > 40%" as a forecasting threshold. But both methods trended to over-predicted this fog event and fogs in some other states. The probability forecast with the present scheme, on the other hand, also fully captured the Gulf coast fog event (Fig.13c), but it had much less over-prediction regions compared to the visibility (Fig. 13a) and multi-rule method (Fig. 13b). Furthermore, the ensemble probabilities for different fog intensities (medium and dense fog) also can be predicted by the present method as shown in Fig. 13d and e.

7. A case study for ice fog in Yellowknife Canada

Ice fog occurs in extreme cold environment (Thuman and Robinson 1954, Girard and Blanchet 2001). Under a very cold condition (below – 20 ^{o}C), the saturation relative humidity should be w.r.t ice surface instead of liquid water surface. Since the saturated vapor pressure w.r.t. ice is much lower than that w.r.t. liquid water, the saturated threshold *RHs* for ice fog is much lower than 100% for warm fog. Such a saturated threshold *RHs* for ice fog in different temperature can be estimated from the curve shown in Fig. 3. Besides the relative humidity, the gravitational settling velocity of crystals in ice fog is also different from liquid droplets in warm fog in that shapes of crystals are different from a sphere (Girard and Blanchet 2001). However, according to aircraft measurements in Germany (Deus 2005,

http://www.ozonesec.ch.cam.ac.uk/scout_o3/meetings/manchester/presentations/De_Reus.pdf) , the terminal velocity of ice crystals within the ice fog mean size range (1~5 μm) is very similar to that of liquid droplets in warm fog. Thus for simplicity, the *LWC* of ice fog can be predicted from a model output data in the same way as warm fog does.

Unlike warm fog, ice fog is rarely measured at high latitude although it is extremely important to aviation in high latitude areas (Alaska and Canada). During November 2010 to March 2011, an ice fog field observation project, FRAM-ICE, at the airport of Yellowknife, North Territory (NT), Canada, was carried out by the Environment Canada (EC). The location is shown in Fig. 14, where ice fog occurs frequently in the winter season. This field project provides a unique opportunity to verify ice fog prediction from NCEP's operational NAM model in high latitude regions in winter time. In this section, an ice fog event occurred on Dec. 17-18, 2010 is used in this study. As was reported by Gultepe of EC (personal communication), this ice fog appeared at midnight of Dec. 17, 2010 and dissipated at noon of next day, Dec. 18, with total duration time about 12 hours. The daytime of Dec. 17 was a clear day with temperature around 20 ^{o}C below zero. From Fig. 3, it can be estimated that the saturation threshold *RHs* for this ice fog was about 85%, much less than warm fog (~100%). During ice fog event, ice crystals were also observed.

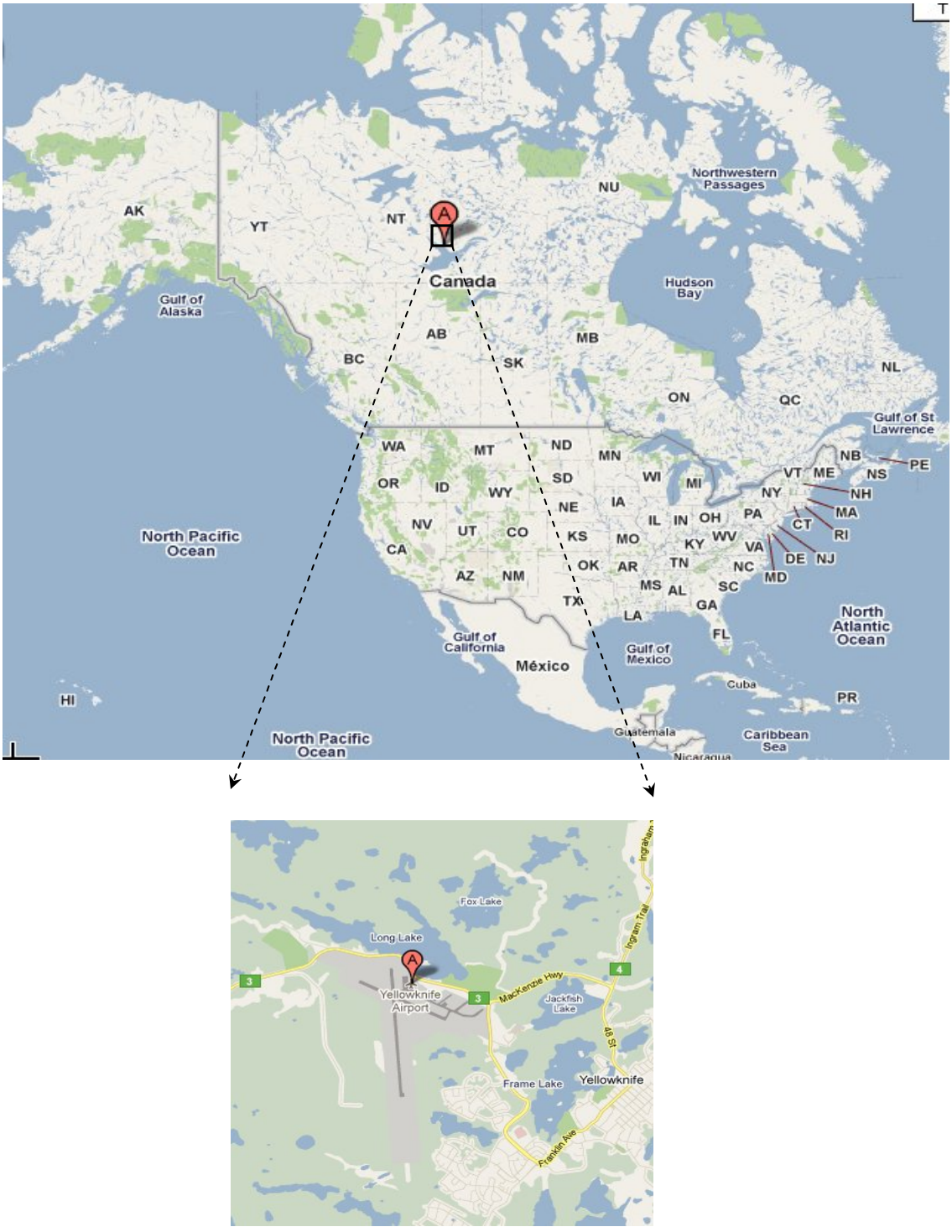

Fig. 14, Yellowknife ice fog observation project (FRAM_ICE) site location

To validate the predictions with 3 different schemes from NAM for this ice fog, the model output data at nearest grid point to Yellowknife airport were selected. Since NAM has 4 runs (00, 06, 12, 18Z) per day out to 87 forecast hours, the run at 18Z (or about 11:00 local time) is presented . Table 5 shows various output variables for the first 25 forecast hours from 18Z NAM run on Dec. 17, 2010. *RHs* values are threshold w.r.t. ice.

Table 5. Model output data from first 25 forecast hours from NAM run at 18Z (local time 11:00 am), Dec. 17, 2010, at nearest grid point to Yellowknife airport. *RH* and *RHs* are relative humidity and saturation relative humidity threshold with reference to ice, respectively. Multi-rule is diagnostic result of fog occurrence with "2m *RH* > *RHs* and wind speed < 2 m/s". The shading in the first column indicates the times of beginning and ending of the ice fog observed.

Forecast hours (local time)	RH_{2m} (%)	***RHs*** (%)	T_{2m} (^{o}C)	**10mWind speed** (m/s)	**Visibility** *(m)*	**Multi-rule**
1 (12:00)	85.0	85.5	-16.7	2.49	4429	No
2 (13:00)	85.8	84.9	-17.0	2.25	4482	No
3 (15:00)	85.5	85.1	-17.8	1.68	4483	Yes
4 (16:00)	91.3	84.3	-18.8	1.32	4531	Yes
5 (17:00)	90.5	83.8	-18.9	1.40	4479	Yes
6 (18:00)	90.8	83.5	-19.7	0.97	4581	Yes
7 (19:00)	91.0	83.3	-20.1	0.68	4583	Yes
8 (20:00)	90.8	82.0	-20.3	0.84	4532	Yes
9 (21:00)	90.3	81.5	-20.4	0.55	4534	Yes
10 (22:00)	90.5	81.3	-20.6	0.48	4625	Yes
11 (23:00)	89.8	80.9	-21.0	1.23	4583	Yes
12 (00:00)	88.0	80.8	-21.2	1.66	4637	Yes
13 (01:00)	87.3	80.7	-21.5	1.62	4631	Yes
14 (02:00)	85.8	80.6	-21.7	1.92	4643	Yes
15 (03:00)	84.3	80.6	-21.6	1.99	4636	Yes
16 (04:00)	84.3	80.7	-21.9	1.91	4632	Yes
17 (05:00)	83.0	80.4	-22.2	2.19	4634	No
18 (06:00)	82.0	80.1	-22.5	2.5	4692	No
19 (07:00)	81.8	79.9	-22.8	2.56	4639	No
20 (08:00)	81.3	79.9	-22.8	2.47	7239	No
21 (09:00)	81.0	79.8	-22.9	2.62	9583	No
22 (10:00)	80.0	79.8	-22.8	2.94	10032	No
23 (11:00)	80.0	79.8	-22.7	3.22	17830	No
24 (12:00)	79.0	80.2	-22.4	3.30	19281	No
25 (13:00)	79.0	80.7	-21.5	3.40	24232	No

If using visibility (6^{th} column) to diagnoses fog, no any fog could be predicted. However if using multi-rule with 2m *RH* > *RHs* and 10m wind speed < 2 m/s to diagnose, fog began after

2 hours forecast (15:00 local time), which was 9 hours earlier than observation and dissipated (04:00 local time) 8 hours earlier than observed time. If using present scheme with temperature, *RH* and wind speeds at surface and upper levels to diagnose fog, the results are improved as listed in Table 6.

Table 6. Diagnostic results with present scheme using NAM's 25 hour forecast output data same as Table 5. The shading in the first column indicates the times of beginning and ending of the ice fog observed. The ice water content (*IWC*) is the value at 10m level.

Forecast hours (local time)	RH_{2m} (%)	*RHs* (%)	H_{sat} (m)	IWC_{10m} (g/kg)	βC_o (g/kg/hr)	*Adv* (g/kg/hr)	*C_Adv* (g/kg/hr)	*K* (m^2/s)	K_c (m^2/s)	*FBL* (m)
1 (12:00)	85.00	85.50	0	0	NA	NA	NA	NA	NA	NA
2 (13:00)	85.80	84.86	62.6	0	0.0421	-0.0335	0.0087	0.8706	0.2638	142.53
3 (15:00)	85.50	85.11	46.2	0	0.0851	-0.0191	0.0660	10.4476	0.4621	720.75
4 (16:00)	91.30	84.25	38.6	0	0.0742	-0.0292	0.0451	8.3308	0.2916	760.97
5 (17:00)	90.50	83.82	44.2	0	0.0363	-0.0191	0.0172	7.5698	0.2208	1045.35
6 (18:00)	90.80	83.45	52.0	0	0.0378	-0.0101	0.0277	6.7604	0.3575	678.54
7 (19:00)	91.00	83.01	43.2	0	0.0267	-0.0140	0.0126	4.9333	0.1828	804.23
8 (20:00)	90.80	81.67	76.8	0.0531	0.0090	0.0004	0.0094	0.0000	0.3739	0.00
9 (21:00)	90.30	81.47	74.7	0.0647	0.0148	-0.0004	0.0144	0.0000	0.4443	0.00
10 (22:00)	90.50	81.25	72.1	0.0764	0.0156	0.0054	0.0210	0.0005	0.5081	0.04
11 (23:00)	89.80	80.93	72.2	0.1034	0.0225	0.0158	0.0384	0.0000	0.6881	0.00
12 (00:00)	88.00	80.84	65.1	0.0585	-0.0006	0.0144	0.0138	0.0000	0.3539	0.00
13 (01:00)	87.30	80.67	59.3	0.0864	0.0183	0.0155	0.0338	0.0000	0.4806	0.00
14 (02:00)	85.80	80.63	61.9	0.0493	0.0022	0.0083	0.0104	0.0000	0.2849	0.00
15 (03:00)	84.30	80.73	66.8	0	-0.0301	-0.0040	-0.0341	NA	NA	NA
16 (04:00)	84.30	80.73	61.8	0.0679	0.0228	-0.0029	0.0199	0.0004	0.3923	0.04
17 (05:00)	83.00	80.41	60.6	0.0549	0.0212	-0.0079	0.0133	0.0002	0.3113	0.03
18 (06:00)	82.00	80.10	58.7	0.0494	0.0205	-0.0094	0.0112	0.0010	0.2721	0.15
19 (07:00)	81.80	79.88	56.1	0.0485	0.0146	-0.0032	0.0114	0.0030	0.2566	0.45
20 (08:00)	81.30	79.88	53.2	0	0.0020	-0.0068	-0.0048	NA	NA	NA
21 (09:00)	81.00	79.79	49.4	0	0.0039	-0.0061	-0.0022	NA	NA	NA
22 (10:00)	80.00	79.81	44.2	0	-0.0005	-0.0068	-0.0073	NA	NA	NA
23 (11:00)	80.00	79.78	44.8	0	-0.0005	-0.0089	-0.0185	NA	NA	NA
24 (12:00)	79.00	80.20	0	0	NA	NA	NA	NA	NA	NA
25 (13:00)	79.00	80.70	0	0	NA	NA	NA	NA	NA	NA

At first forecast hour, surface has not saturated ($RH < RHs$ and $H_{sat} = 0$ in first row in Table 6), so fog did not form yet. From 2 to 7 hours of forecast, surface layer saturated ($RH > RHs$) with saturated depth H_{sat} about 40 ~ 60 m, but still no fog appeared due to very large

turbulence intensity ($K >> K_c$) although during this time total ice water generation rate was positive. During this period, positive cooling ice water generation rate exceeded ice water reduction rate due to dry advection. However, the cooling generated ice water failed to accumulate due to large turbulence as expressed by *K*. After 8 forecast hours (or 20:00 local time), turbulence rapidly decreased to zero due to intensified surface inversion and continuous cooling of the surface. At this time, total ice water generation rate also increased in response to sign change of advection term (from negative to positive, i.e. from dry to wet advection). The increase in total ice water generation led to a larger K_c as shown in Eq. 9. An increasing K_c and a ceasing *K* led to "$K < K_c$" so that ice fog formed as indicated by $IWC \sim 0.0531\ \mathrm{g}\,kg^{-1}$ at 20:00 local time. This ice fog onset time was 4 hours earlier than observation reported by Gultepe (personal communication) as shown with shading cells in the first column. The diagnostic *IWC* of this ice fog reached its maximum, 0.1034 g kg^{-1} , with fog depth about 70m at 23:00 local time. From this time on, decrease in both *IWC* and fog depth, due to reduction in both cooling and moisture advection generation was observed. At 15 forecast hours (03:00 local time), the fog disappeared temporally due to warming and dry advection. One hour later (16 forecast hours), the ice fog resumed and persisted until it dissipated at 19 forecast hours (or 07:00 local time). The dissipation time was also 4 hours earlier than that observed. But total fog duration time, around 12 hours, is close to the observation. The fog dissipation was not caused by warming but by dry advection after 07:00 local time. Between 07:00 to 09:00 local time, surface still showed cooling. Only after 10:00, surface cooling changed to warming most likely due to sunrise, after which fog speeded to burnout with its depth rapidly decreasing. After 12:00 local time, surface *RH* was less than its *RHs* threshold (w.r.t. ice) and the saturated layer completely dissipated (H_{sat} = 0), which was comparable to the reported fog dissipation time. The last column shows the *FBL* values at all forecast hours. It can be found that after surface saturated but before fog appeared (i.e. $H_{sat} > 0$ but IWC = 0), *FBL* was still higher than *Has*. After fog formed, the *FBL* was much lower than fog depth (H_{sa}). Since there is no further *K,* K_c and *FBL* computations after the scheme detects no positive water generation, "NA" is given to these values (15, 20,21,22,23 forecast hours) Similarly, there is no further βC_o**,** *Adv, C_Adv***,** *K,* K_c, and *FBL* computations after the scheme detects no saturation, NA is set to these parameters in the first and last 2 rows in Table 6.

Another interesting feature in Table 6 is that the saturated layer existed ($H_{sat} > 0$) but no fog formation ($IWC = 0$) during initial forecast hours (from 13:00~19:00) and in the last a few hours (from 08:00 ~ 11:00). This means that even when the surface air has saturated, fog may not form due to not strong cooling or too strong turbulence intensity. This confirms the fact that saturation air is only a necessary, not a sufficient condition for fog. Such a phenomenon is very similar to what is called "*near-fog*" condition by Bergot et al (2009). In real world, this condition may be equivalent to conditioning stage of fog (Meyer, et al 1986) , or light fog (defined as visibility > 1000 m but < 2000m by NWS) or haze.

8. Summary

Based on an asymptotic analysis of radiation fog by Zhou and Ferrier (2008), a new fog diagnostic scheme in model post processor has been proposed by extending it to include moisture advection and cloud top and base. The scheme diagnoses grid-scale fog liquid water content (*LWC*) from surface and vertical temperature, *RH*, winds, etc. basic variables by checking three necessary conditions: (i) existence of surface saturated layer or low cloud layers; (ii) positive *LWC* generation rate, either by cooling, or by moisture advection or by the both; and (iii) turbulent exchange coefficient smaller than its critical value. Only when all these three conditions are satisfied at same time, has fog at this grid and can its *LWC* be computed. The scheme is executed in following steps: (1) check if model cloud top and base are less than certain level, if yes, it is low stratus or cloud subsidence fog. In this case, the model cloud depth is set as fog depth. (2) If it is not the case, level-by-level search depth of saturation layers on the ground upward. If no surface cloud or no saturated layer exists, return 0 *LWC*, otherwise, (3) further compute total fog water generation rate by cooling and moist advection. If the total fog water generation is negative, return 0 *LWC*, otherwise, (4) further compute *Ri* number followed by computing turbulent exchange coefficient *K* and its critical value K_c. If $K > K_c$, return 0 *LWC*, otherwise (5) compute *LWC* vertical distribution. Using 10m *LWC* as surface *LWC* as final output.

It has been implemented and tested in some of NCEP's mesoscale models and ensemble forecast system. In this document, fog predictions by this scheme and other 2 methods

conducted in the post processors of RUC, NCAR-ARW WRF and VSREF system for Nov. 2010 Gulf coast fog are compared, showing that the new scheme has better performance for this particular coast fog in comparison to visibility and multi-rule diagnostic methods from the same models in terms of correct forecast fog event areas and less false alarms. To show its capability of prediction for ice fog, prediction by this scheme in NAM post processor for ice fog event on Dec. 17~18 in Yellowknife of Canada is also presented, showing that the prediction with this scheme can generally represent the Yellowknife ice fog event although its onset and ending times are predicted a few hours earlier than observations. If with visibility method, no ice fog could be diagnosed while if with multi-rule method, its onset and ending times will be much earlier than observations.

It is noted that the asymptotic analysis theory (ZF08) is a approximate formulation with curtain accuracy and application scopes. Although limited verifications for this scheme show promising result in comparison to other 2 diagnostic methods, complete verification with large amount of fog data has not been conducted, partly due to a lack of direct observation data in fog events. To fully understand the performance of the new fog scheme, our future work will focus on further verifications with available fog data, particularly from METAR and ADDS data set.

Acknowledgement. Grateful to Drs. Mike Ek and Jianping Huang of EMC for their reviewing of the original manuscript. Their valuable comments and suggestions greatly improved the final edition of this report. The Yellowknife ice fog event data used in validation in this document were obtained in the FRAM-ICE observation project and provided by Dr. Gultepe of Environment Canada. The ADDS data and METAR data used in Nov. 23-24 Gulf coast fog event were downloaded from NCEP-AWC web site http://aviationweather.gov/adds.

Appendix

Testing code for this scheme (in Fortran 77/90, which can be compiled and standalone run at Linux or other Unix platforms) and one testing sample data can be downloaded from ftp://ftp.emc.ncep.noaa.gov/mmb/bzhou/New_fog_scheme

Reference

Beare R. and coauthors, 2006: An intercomparison of large-eddy simulation of the stable boundary layer, Boundary-Layer Meteor., **118**, 247-271.

Beljaars, A., 1992: The parameterization of the planetary boundary layer, ECWMF, Report May 1992, available online http://www.ecmwf.int/newsevents/training/rcourse_notes/ PARAMETRIZATION/BOUNDARY_LAYER/Boundary_layer4.html

Bergot, T. and D. Guedalia, 1994: Numerical forecasting of radiation fog. Part I: Numerical model and sensitivity tests. *Mon. Wea. Rev*., **122**, 1218-1230.

_____, D. Carrer, J. Noilhan and P. Bougeault, 2005: Improved site-specific numerical prediction of fog and low clouds. A feasibility study. *Wea. Forecasting*, **20**, 627-646.

Bott, A., U. Sievers, and W. Zdunkowski, 1990: A radiation fog model with a detailed treatment of the interaction between radiative transfer and fog microphysics. *J. Atmos. Sci*., **47**, 2153-2166.

Brown, R. and W. T. Roach, 1976: The physics of radiation fog: II – a numerical study. *Quart. J. Roy. Meteor. Soc*., **102**, 335-354.

Businger, J. A., J. C. Wyngaard, Y. Izumi and E. F. Bradley, 1971: Flux profile relationships in the atmospheric surface layer. *J. Atmos. Sci*., **28**, 181-189

Girard, E., and J.-P. Blanchet, 2001: Simulation of arctic diamond dust, ice fog, and thin stratus using an explicit aerosol-cloud-radiation model. *J. Atmos. Sci.,* **58**, 1199-1221.

Guedallia, D. and T. Bergot, 1994: Numerical forecasting of radiation fog, Part II: A comparison of model simulation with several observed fog events. *Mon. Wea. Review*, **122**, 1231-1246

Kunkel, B. A., 1984: Parameterization of droplet terminal velocity and extinction coeffi-cient in fog models. *J. Climate Appl. Meteor*., **23**, 34-41.

Mellor, G. L. and T. Yamada, 1974: A hierarchy of turbulence closure models for planetary boundary layers. *J. Atmos. Sci*., **31**, 1791-1806.

Meyer, M. B., G. G. Lala, and J. E. Jiusto, 1986: Fog-82: A cooperative field study of radiation fog. *Bull. Amer. Meteor. Soc*., **67**, 825-832

Müller, M. D., M. Masbou, A. Bott, and Z. Janjic, 2005: Fog prediction in a 3D model with parameterized microphysics. Preprints, *World Weather Research Programme's Symposium on Nowcasting and Very Short Range Forecasting*, September 5-9, Toulouse, France.

Musson-Genon, L., 1987: Numerical simulation of a fog event with a one-dimensional boundary layer model. *Mon. Wea. Review*, **115**, 592-607.

Nakanishi, M., 2000: Large-eddy simulation of radiation fog. *Boundary-Layer Meteorol*. **94**, 461-693.

Pagowski, M., I. Gultepe, and P. King, 2004: Analysis and modeling of an extremely dense fog event in southern Ontario. *J. Appl. Meteor*., **43**, 3-16.

Peterssen (1940): *Weather Analysis and Forecasting*, McGraw-Hill, New York and Landon, 505pp.

Roach , W. T., R. Brown, S. J. Caughey, J. A. Garland and C. J. Readings, 1976: The physics of radiation fog: I – a field study. *Quart. J. Roy. Meteor. Soc*., **102**, 313-333

Shi, C., and coauthors, 2010: Analysis of an extremely dense regional fog event in eastern China using a mesoscale model. *Atmos. Res*, **95**, 428-440.

Stoelinga, M. T. and T. T. Warner, 1999: Nonhydrostatic, mesobeta-scale model simulations of cloud ceiling and visibility for an east coast winter precipitation event. *J. Apply. Meteor*., **38**, 385-404.

Stull, R. B., 1988: An *Introduction to Boundary layer Meteorology*, Kluwer Academic Publishers, 666 pp.

Thuman, W. C., and E. Robinson, 1965: Studies of Alaska ice fog particles, *J. Meteor*., **11**, 151-156.

Van Dyke, M. D., 1964: *Perturbation Methods in Fluid Mechanics*. New York, Academic Press, 229 pp.

Van der Velde, I. R., G. J. Steeneveld, B. G. J. W. Schreur, and A. A. M. Holstlag, 2010: Modeling and forecasting the onset and duration of severe radiation fog under frost conditions. *Mon. Wea. Rev*., in press.

Welch, R. M., M. G. Ravichandran, and S. K. Cox, 1986: Prediction of quasi-periodic oscillations in radiation fogs. Part I: Comparison of simple similarity approaches. *J. Atmos. Sci*, **43**,633-651.

WMO (2008): *Guide to Meteorological Instruments and Methods of Observation (CIMO Guid*e)

Zhao. L, S. Niu, Y. Liu, C. Lu, J Lü, and J.Yang, 2010: Impact of Turbulence on Radiation Fog . *5th International Fog, Fog Collection and Dew Conference*, Münster, Germany , Special Issue.

Zhou, B. and B. S. Ferrier, 2008: Asymptotic analysis of equilibrium in radiation fog. *J. Appl. Meteor. and Clim*., **47**, 1704-1722.

____, B. and J. Du, 2010: Fog prediction from a multimodel mesoscale ensemble prediction system, *Wea. Forecasting*, **25**, 303-322.

____, B., J. Du, I. Gultepe and G. Dimego, 2011: Forecast of Low Visibility and Fog From NCEP– Current Status and Efforts, *Pure and Appl. Geophys*., in press.